Earth and Planetary Science Letters 605 (2023) 118039

Contents lists available at ScienceDirect

Earth and Planetary Science Letters

journal homepage: www.elsevier.com/locate/epsl

Onset of convection from hydrate formation and salt exclusion in marine sands

David Fukuyama [a,b,*], Hugh C. Daigle [a], Michael A. Nole [b], Wen Song [a]

[a] Hildebrand Department of Petroleum and Geosystems Engineering, 200 E. Dean Keeton St., Stop C0300, Austin, 78712, TX, USA
[b] Sandia National Laboratories, Albuquerque, 87185, NM, USA

ARTICLE INFO

Article history:
Received 10 October 2022
Received in revised form 25 January 2023
Accepted 31 January 2023
Available online xxxx
Editor: L. Coogan

Keywords:
methane hydrate
density-driven flow
convection

ABSTRACT

Short-range diffusion and long-range advection are two endmember mechanisms responsible for transporting methane to locations suitable for hydrate formation in the subsurface. This study introduces a novel transport mechanism in natural porous media: density-driven convection of pore fluids due to hydrate formation and salt exclusion in the pore water. Geologic hydrate systems simulations typically consider the role of salt only as it impacts the equilibrium phase behavior, but have largely ignored its effect on density and mobility impacting fluid flow. In a system sourced with microbially-generated methane, as methane enters a brine-saturated sand from an overlying clay layer, convection is initiated by hydrate formation from methane and water, which excludes salt and thereby increases the salinity of the remaining pore water. As the pore water becomes more saline, the density increases, causing a gravitational instability as the more saline, denser fluid layer overlies a less dense fluid. Fluid parcels are then dragged throughout the layer at a rate as high as 3 cm/yr, which distributes aqueous methane throughout the layer, reaching solubility on a shorter timescale than by diffusion alone. In this study, we examine the factors affecting convection and its ability to transport methane in a layered clay-sand system. We demonstrate the rapid transport of aqueous methane throughout the sand layer with convection compared with diffusion, and how the convective velocity increases with increased hydrate saturation formation rates. The relatively fast rate of convective transport makes convection a viable transport mechanism for supplying deeper sediments with methane generated in shallow regions.

1. Introduction

Several methane transport mechanisms have been proposed to account for the supply of geologic systems with the necessary molecular components to form hydrate within sands. Short-range diffusion of aqueous methane from sand-adjacent clays, and long-range advection of methane gas from a deeper source are two endmember transport mechanisms that supply sand layers with methane (You et al., 2019). Diffusion alone is insufficient to fill thick (m scale) sands completely with hydrate (Nole et al., 2017), thus an alternate transport mechanism for supplying methane to these sands must exist. Overpressure-driven methane migration (Nole et al., 2016) and compaction-driven fluid flow (Frederick and Buffett, 2011) are two fluid-focusing mechanisms of methane transport that supply methane from greater depths and higher methane solubilities towards shallower regions with lower methane solubilities. Advective methane flux allows for higher hydrate saturations than diffusive flux alone, due to the faster rate of mass transfer. We propose a new transport mechanism for aqueous methane: convection initiated by hydrate formation and subsequent salt exclusion in the pore water.

Geologic systems consisting of alternating layers of fine- and coarse-grained lithologies commonly host high hydrate saturations within the coarse-grained sand layers (Malinverno et al., 2008; Malinverno and Goldberg, 2015). Pore radius dictates the solubility of aqueous methane due to the Gibbs-Thomson effect (i.e. larger curvature in small pores gives rise to increased methane pressure), with solubility of methane in the aqueous phase scaling with the logarithm of the inverse of the pore radius (Henry et al., 1999; Liu and Flemings, 2011). This solubility contrast between the fine- and coarse-grained layers is an important parameter for determining the diffusive mass flux of methane out of the fine-grained layers where it is generated by microbial consumption of organic matter, to the coarse-grained layers, where it forms hydrate. Since the solubility of methane is higher in the fine-grained layers (Henry et al., 1999), as microbially-generated methane is produced, the methane concentration increases without forming hydrate and subsequently

* Corresponding author.
E-mail address: fukuyama@utexas.edu (D. Fukuyama).

https://doi.org/10.1016/j.epsl.2023.118039
0012-821X/

diffuses along the concentration gradient to a region of lower solubility in the coarse-grained layers, where it can form hydrate (Malinverno, 2010). Diffusive methane transport is capable of filling thin sand layers adjacent to thick clay layers with high hydrate saturations (Malinverno and Goldberg, 2015), but is largely insufficient for fully saturating thick sand layers with hydrate, as the majority of the hydrate will form at the outer edge of the sand layer, with lower hydrate saturations within the interior of the layer (Rempel, 2011).

Long-range migration of methane, dissolved in the pore fluid or in the gas phase, has been proposed as a method whereby greater accumulations of hydrate can form within coarse-grained layers than with purely diffusive transport of methane. Advection of fluids by compaction-driven flow (Frederick and Buffett, 2011) or through overpressure (Nole et al., 2016) can focus high concentrations of dissolved methane through permeable, coarse-grained layers, resulting in hydrate formation as solubility decreases towards the seafloor. Free gas flow can similarly form hydrate within thick sands, as salt excluded by hydrate formation allows the coexistence of gas and hydrate (You and Flemings, 2018). While free gas flow can provide high hydrate saturations in these coarse-grained layers, the geochemistry of many hydrate systems including those in the Nankai Trough (Waseda and Uchida, 2004), Ulleung Basin (Choi et al., 2013), and the Krishna-Godavari Basin (Tripathi et al., 2019) indicates methane of microbial origin, which is largely associated with generation at shallow depths and existence in the aqueous phase. While microbial gas can be generated at greater depths and migrate buoyantly as a gas phase, microbial methane generated in the clays adjacent to coarse-grained sands will remain in the dissolved phase due to relatively low generation rates.

The convective transport of aqueous methane introduced in this study combines aspects of diffusive transport of methane with advective liquid transport. Convection and advection are often used interchangeably when discussing flow in porous media, but in the context of our work, free convection describes flow occurring from a driving force of density gradients rather than pressure, and advection describes the transport of a dissolved component by fluid motion. In our study, methane diffusively enters the sand layer following microbial generation in a fine-grained clay layer adjacent a coarse-grained sand layer. As the methane concentration surpasses its saturation limit in the sand layer, hydrate forms and removes aqueous methane and water, leaving salt in the pore fluids. Hydrate saturation increases from the continual flux of microbially-generated methane, and the excluded salt increases the salinity of the pore water. In a system with a sufficiently high methane supply rate, hydrate will form at a rate faster than the salt can diffuse. The denser, more saline pore water overlying the less dense, less saline pore water below will develop a convective instability and drag the denser fluid parcel, including the dissolved methane, down into the sand layer. We find that density-driven convection is capable of transporting clay-generated methane through permeable sands on the order of cm/yr.

2. System definition

Hydrate deposits are commonly found in geologic systems with thick sands interbedded between clays. These depositional environments include mass transport deposits in the Alaminos Canyon 21 region (Boswell et al., 2012), channel-levee deposits in Green Canyon 955 (Flemings et al., 2020) of the Gulf of Mexico, and turbidite sands in the Nankai Trough (Ito et al., 2015). Microbial methanogenesis has been proposed as a source of methane generation in these systems, where the low ratio of ^{13}C to ^{12}C ($\delta_{13}C < -60‰$) and high ratio of methane to heavier hydrocarbons ($CH_4/(C_2H_6+C_3H_8)>1000$) of these systems is largely consistent with a microbial methane source (Malinverno et al., 2008). Due to their rapid deposition, relatively small quantities of total organic carbon (TOC) are deposited with the sands. Methane is therefore mainly generated in the clays, as they contain higher quantities of TOC. The mass flux of methane out of the clays and into the sands is limited by the pore size contrast, rate of microbial conversion of organic matter to methane, and thickness of the clay layer adjacent to the sand (Cook and Malinverno, 2013). Methane flux into the sands from methane generated microbially within the clays is therefore maximized with a thick clay and a large contrast between the median clay and sand pore radii (Fukuyama and Daigle, 2020). High hydrate saturations in these sands are achievable on the outer edges of the sand body, but large hydrate accumulations throughout the entirety of the sand body are limited by the rate of diffusive methane transport (Nole et al., 2017; Rempel, 2011).

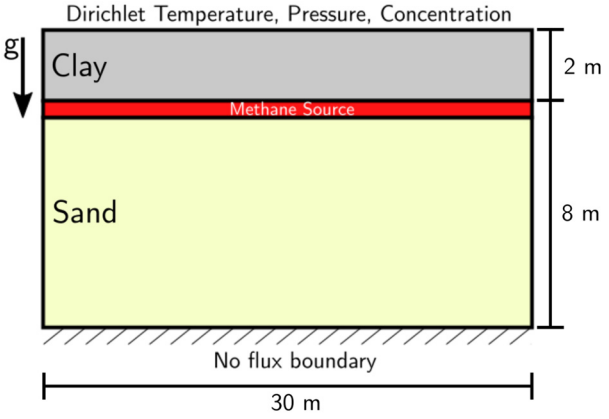

Fig. 1. The system used in this study is a clay layer overlying a sand layer with a Dirichlet pressure, temperature, and concentration boundary above, and a no-flux Neumann boundary below. A line source was set through the top of the sand layer to represent the flux of methane from a thick clay layer.

In the numerical simulation here, the system and boundary conditions replicate the key elements of a thick sand layer supplied with microbially-generated methane from a bounding clay layer (Fig. 1). The constant flux of microbially-generated methane into the sand was modeled as a line source of methane through the uppermost gridblock of the sand layer. A line source representing the methane flux ranging from $1.7 \cdot 10^{-13}$ kg m^2 s^{-1} to $1.7 \cdot 10^{-12}$ kg m^{2}s^{-1} was used rather than discretizing the entire overlying clay body to improve the overall computational efficiency of the simulation. Dirichlet boundary conditions of pressure, temperature, and mole fraction of methane and salt were imposed on the upper boundary of the clay equal to initial conditions, and a no-flux Neumann boundary condition of mass and energy was imposed on the bottom of the sand and the left and right sides of the domain. The uppermost Dirichlet boundary does not provide the system with methane, but rather serves as a pressure boundary to reduce the pressure effects that arise when adding mass to the system through a source term. Heat transfer at the boundary is considered through a Dirichlet temperature boundary condition along the top of the domain, and a zero-flux energy boundary at the bottom.

The system was initialized at a pressure of 30 MPa, and a constant temperature of 2 °C without a geothermal gradient. Because the simulated sand layer was relatively thin (8 m), a geothermal gradient was not applied. Gridblock sizing was set to 0.25 m in x and y, following the criterion described by Hassanzadeh et al. (2007), that suggests gridblock spacing be 20 times smaller than the initial wavelength of the convective instabilities. This discretization ensures that the convective cells are properly resolved.

Both solutes were assumed to have the same diffusion coefficient of $3 \cdot 10^{-10}$ m^2/s (You and Flemings, 2018). Clays typically have a more tortuous pathway of diffusion than the sands due to

Table 1
Simulation parameters used in the clay and sand layers.

Parameter	Clay	Sand
Porosity [−]	0.40	0.40
Permeability [m^2]	$1 \cdot 10^{-18}$	$5 \cdot 10^{-13}$
Median pore diameter	50 nm	10 μm
Tortuosity	0.05	0.5
Rock density	2700 kg m^{-3}	
Rock thermal conductivity	1.1 W m^{-1}C^{-1}	
Rock heat capacity	830 J kg^{-1}C^{-1}	
Solute diffusion coefficient	$3 \cdot 10^{-10}$ m^2 s^{-1}	
Initial salt concentration [mole frac.]	0.02	
Initial methane concentration [mole frac.]	0.0	
Gridblock size [m]	0.25×0.25	

the higher aspect ratio of clay pores (Daigle and Dugan, 2011). Due to the effects of tortuosity, the effective diffusivity of dissolved components is lower within the clays than within the sands, which slows the diffusion of methane through the clay. Clay permeability was set to 10^{-18} m^2 and sand permeability was set to $5 \cdot 10^{-13}$ m^2, values typical of hydrate-bearing sediments in the northern Gulf of Mexico (Daigle et al., 2015). The relevant simulation parameters are displayed in Table. 1.

3. Simulation methods

We use an extension of PFLOTRAN, a massively parallel reactive flow and transport simulator (Hammond et al., 2014), to track hydrate formation and component transport. Hydrate formation in PFLOTRAN assumes thermodynamic equilibrium, and therefore phase transitions are assumed to be instantaneous. PFLOTRAN implicitly solves mass balance equations for water, methane and salt that take the following form:

$$\frac{\partial}{\partial t}\phi \sum_{\alpha=l,\,h}\left(s_\alpha \rho_\alpha x_j^\alpha\right) + \nabla \cdot \left(\boldsymbol{q}_l \rho_l x_j^l - \phi s_l D_l \rho_l \nabla x_j^l\right) = Q_j, \tag{1}$$

where ϕ is porosity, α is the pore-filling phase (liquid or hydrate), s is the phase saturation, ρ is the phase density, x_j^α is the mole fraction of component j ($j = H_2O, CH_4, NaCl$), q is the Darcy flux, D is the solute diffusion coefficient, and Q is the component source term. The Darcy flux of the liquid phase is defined as

$$\boldsymbol{q_l} = -\frac{k k_{rl}}{\mu_l}\nabla(P_l - \rho_l \boldsymbol{g} z), \tag{2}$$

where k is the intrinsic permeability of the rock, k_{rl} is the relative permeability of the liquid phase, μ_l is the viscosity, P_l is the liquid phase pressure, ρ_l is the liquid phase density, g is the gravitational constant, and z is the depth in the direction of gravity.

An energy balance equation is also solved:

$$\sum_{\alpha=l,h}\left(\frac{\partial}{\partial t}(\phi s_\alpha \rho_\alpha U_\alpha + \nabla \cdot (\boldsymbol{q_\alpha}\rho_\alpha H_\alpha)\right) + \frac{\partial}{\partial t}\left((1-\phi)\rho_r C_p T\right) - \nabla \cdot (\kappa \nabla T) = Q \tag{3}$$

where U represents the internal energy, H represents the enthalpy, C_p represents the heat capacity of the rock, and κ represents the thermal conductivity of the rock. The energy balance equation considers contributions from the pore-filling liquid (l), and hydrate (h) phases, as well as the rock (r) matrix.

Heat transfer to the surrounding formations is simulated through the energy balance equation (Eq. (3)). The formation of hydrate is exothermic, and the enthalpy of hydrate is computed as a function of temperature (Handa, 1986):

$$H_h = C_{PH}(T - T_f) + \frac{H_{H0}}{N_H + 1}, \tag{4}$$

where H_h represents the hydrate enthalpy, C_{PH} is the hydrate heat capacity, T is the temperature, T_f is the freezing temperature of water, H_{H0} is the reference hydrate enthalpy, and N_H is the hydration number of hydrate. The hydrate heat capacity is defined as:

$$C_{PH} = 1.620(MW_{H_2O}N_H + MW_{CH_4}), \tag{5}$$

where MW_{H_2O} and MW_{CH_4} are the molecular weights of water and methane, respectively.

The relationship between aqueous methane solubility and pore size is implemented in PFLOTRAN using a capillary pressure-saturation function, $P_c(S_w)$, with a modification to the Gibbs-Thomson equation:

$$\Delta T_G = \frac{T P_c}{H_f \rho_H}, \tag{6}$$

where ΔT_G is the temperature shift to the three-phase equilibrium curve at a given pressure due to the Gibbs-Thomson effect, H_f is the latent heat of fusion of hydrate (54.4 kJ/mol) (Waite et al., 2009), and ρ_H is the hydrate density. This elevates aqueous methane solubility and equilibrium temperature according to the capillary pressure curve assigned to the given lithology.

The Gibbs-Thomson effect restricts hydrate formation in the fine-grained clay layer through an elevated solubility, and promotes hydrate formation within the coarse-grained sand layer. Since the energy-minimizing arrangement of the hydrate phase forms hydrate in the largest pores first, the Gibbs-Thomson effect increases the solubility of methane as the hydrate saturation increases and hydrate forms in smaller pores.

Hydrate is considered an immobile, pore-filling phase that reduces the relative permeability of the liquid water phase. We find the relative permeability using the Van Genuchten-Mualem model (Van Genuchten, 1980):

$$k_{rl} = \sqrt{s_e}\left\{1 - \left[1 - (s_e)^{1/m}\right]^m\right\}^2, \tag{7}$$

where k_{rl} is the relative permeability of the liquid phase, m is a fitting parameter, and the effective water saturation, s_e, is defined as

$$s_e = \frac{s - s_r}{s_0 - s_r}, \tag{8}$$

where s is the water saturation, s_0 is the maximum water saturation, and s_r is the residual water saturation.

The aqueous phase density was computed as a function of salt concentration, pressure, and temperature (Batzle and Wang, 1992), where ρ_W (Eq. (9)) and ρ_B (Eq. (10)) are the water and brine densities (g/cm^3), S is the weight fraction of NaCl (ppm/10^6), P is pressure in MPa, and T is temperature in °C. Water and brine density are given by Batzle and Wang (1992):

$$\rho_W = 1 + 1 \cdot 10^{-6}(-80T - 3.3T^2 + 0.00175T^3 + 489P - 2TP + 0.016T^2P - 1.3 \cdot 10^{-5}T^3P - 0.333P^2 - 0.002TP^2 \tag{9}$$

$$\rho_B = \rho_W + S(0.668 + 0.44S + 1 \cdot 10^{-6}(300P - 2400PS + T(80 + 3T - 3300S - 13P + 47PS))) \tag{10}$$

To probe the impact of convection in geologic systems, we varied the rate of the methane source to reflect mass flux changes arising from varied clay layer thickness and pore size contrast. With this variation, we examined the time to the onset of convection, the characteristics of hydrate formation at the sand-clay interface, the velocity at which methane is transported throughout the system, and the form that the instability takes.

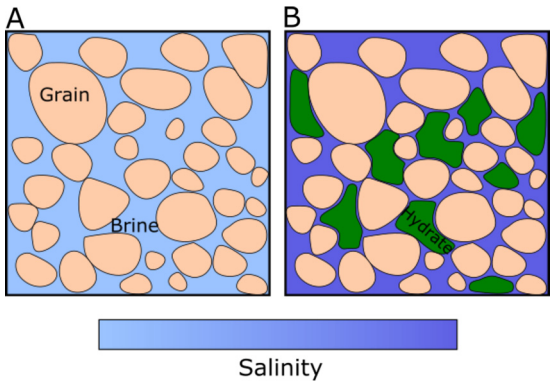

Fig. 2. Salinity increases within the pore water as hydrate is formed due to salt exclusion from the hydrate phase.

4. Stages of convection

Convection is initiated during hydrate formation when the salinity in the surrounding pore water has increased to develop a density contrast high enough to develop an instability. We begin by demonstrating the effect of hydrate formation in a simple, conceptual example that ignores fluid flow (Fig. 2). The system is initialized with methane and salt dissolved in the pore water (Fig. 2A). As hydrate forms from only methane and water, salt is excluded from the hydrate crystal structure and remains dissolved in the surrounding pore water (Fig. 2B). Here, hydrate formation does not completely consume the dissolved methane, and only the methane in excess of solubility forms hydrate. Salt exclusion is tracked through the mass balance equations (Eq. (1)). Because mass is conserved, as hydrate forms, the pore fluid salinity increases due to the mass of dissolved salt remaining constant in the pore fluids while water and methane are consumed by hydrate formation. The increase in salinity raises the density of the pore water, and when a denser fluid such as this overlies a less dense fluid, a convective instability develops and convection begins. Although the formation of hydrate is an exothermic process, the slight temperature increase observed here ($< 0.1\,^{\circ}C$) does not significantly change the fluid density.

In a system with a $6.7 \cdot 10^{-13}$ kg/m^2 s flux of methane into the sand, the formation of hydrate leads to a slightly elevated salt concentration, as well as a slightly more dense fluid at the sand-clay interface (Fig. 3, t = 2000 yr). As hydrate continues to form, the density contrast increases between the higher-salinity pore water at the top of the sand layer and the lower-salinity pore water throughout the rest of the layer until instabilities begin to form (Fig. 3, t = 2500 yr). This convective instability initiates at a hydrate saturation of 17%. The instabilities continue to develop as distinct fingers that drag the denser fluid downward (Fig. 3, t = 2800 yr), along with dissolved methane. As convective flow continues to disperse salt and dissolved methane throughout the layer and the lighter buoyant brine is forced upward, a second instability forms (Fig. 3, t = 3500 y), leading to further advective mixing throughout the layer (Fig. 3, t = 4400 yr). The convective flow continually drags methane at concentrations closer to its saturation limit throughout the sand layer. As the fluid parcels reach the bottom of the layer, the fingers gradually move and combine, forming new convection cells.

5. Comparing diffusion-dominated systems with convection-dominated systems

In diffusion-dominated systems without density-driven convection, methane diffuses from the fine-grained layer where it is generated to the coarse-grained layer where it forms hydrate. Hydrate forms first at the interface between the fine- and coarse-grained layers, and gradually forms towards the center of the layer as hydrate fills the largest pores. The rate of methane generation within the bounding clay layers is dependent on depth, quantity of metabolizable organic carbon, and rate of microbial methanogenesis (Malinverno, 2010). Malinverno (2010) constrains the microbial methanogenesis rate within fine-grained sediments to an upper limit of $5 \cdot 10^{-13}$ kg m^{-3} s^{-1}. Rates as high as $7 \cdot 10^{-13}$ kg m^{-3} s^{-1} have been found at Hydrate Ridge (Claypool et al., 2006), offshore Oregon. The rate of methane flux out of the fine-grained layer and into the coarse-grained layer is a function of the clay layer thickness, the pore size contrast between the fine- and coarse-grained layers, and the rate of microbial action (Fukuyama and Daigle, 2020). These parameters define the shape of the dissolved methane concentration curve, the slope of which determines the flux into the sand. For example, a 10 m thick clay layer with a median pore size of 10 nm generating methane at a rate of $0.37 \cdot 10^{-12}$ kg/m^3 s will generate a diffusive flux of $4 \cdot 10^{-12}$ kg/m^2 s into a sand layer with a 100 μm median pore size (Fukuyama and Daigle, 2020). Using the parameters at Walker Ridge Block 313 Hole H (Cook and Malinverno, 2013), we can estimate the diffusive flux of methane into a 2.5 m sand layer between $2.5 \cdot 10^{-12}$ kg/m^2 s and $5.1 \cdot 10^{-12}$ kg/m^2 s. We use these values as upper limits on the diffusive flux in this study.

The enhancement to methane transport via salt exclusion and density-driven flow, in comparison with current models where methane transport is diffusion-controlled, is illustrated in Fig. 4. In our simulations, both cases are in a purely diffusive regime as hydrate formation begins. When enough hydrate has formed to generate a density-driven instability in the brine, however, the transport of methane throughout the layer increases at a faster rate than the purely diffusive rate (Fig. 4B, $6.7 \cdot 10^{-13}$ kg m^{-2} s^{-1} t = 2700 yr). In systems with a lower methane flux (Fig. 4B, $1.7 \cdot 10^{-13}$ kg m^{-2} s^{-1}), hydrate formation is slow, which limits changes to local salinity. In this case, diffusive mixing of the excluded salt with the surrounding pore waters limits the formation of convective fingers, and the overall mixing converges to the diffusive case. For cases with a high methane flux, however, the onset of density-driven flow transports methane throughout the sand faster than diffusion alone, and a larger fraction of the methane is converted to hydrate. That is, at the same mass flux, the density-driven flow here enables the transport of methane-saturated brines to reach the bottom of the sand layer more rapidly than by diffusion alone.

Within the hydrate stability zone, the highest rates of microbial methane generation are typically found at shallower depths (Malinverno, 2010), where large quantities of labile organic matter are available for microbial conversion of into methane. This indicates that convection is most likely to occur at the shallower depths, where the mass flux of methane out of the clays and into the sands is the highest, while at greater depths, methane mass transfer is mainly diffusive.

Diffusive and convective regimes also differ in the hydrate distribution patterns within the sand layers. While both systems see the bulk of the hydrate formed at the interface between the fine- and coarse-grained layers (Fig. 5A and B, 5000 yr), at t = 22000 yr, hydrate begins to form within the fingers in the convective case, but remains largely confined to the interface in the diffusive case. The fraction of sand containing hydrate (Fig. 5C) shows the difference in the fraction of the sand layer that hosts hydrate between the convective and diffusive cases. Both exhibit similar initial hydrate formation, but at 20000 yr, a majority of the sand layer in the convective cases begins to form hydrate, while the diffusive case is confined to gradual increases in hydrate formation as diffusion brings regions near the interface to solubility.

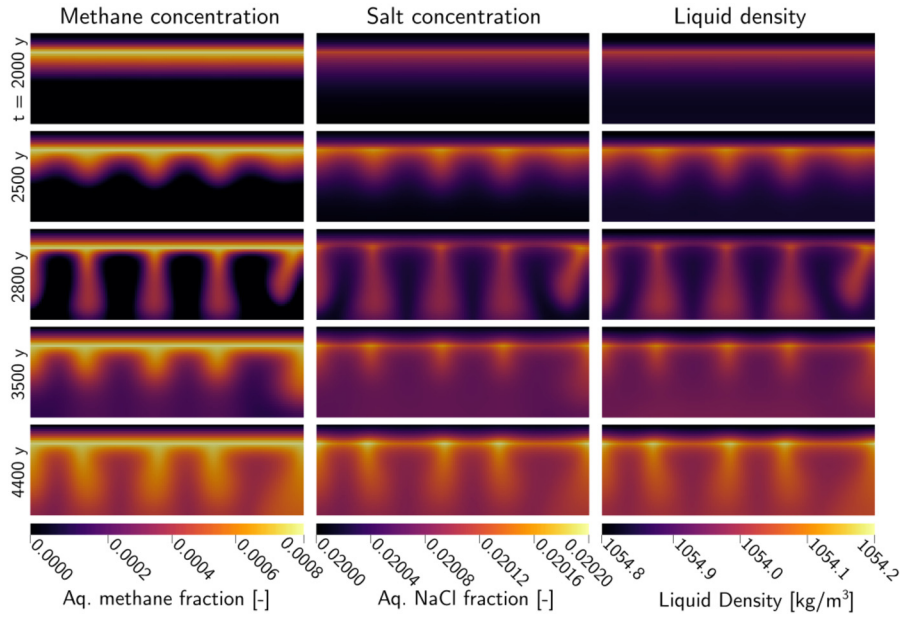

Fig. 3. As hydrate forms at the sand-clay interface, the fluid at the top of the sand layer becomes denser. The higher density fluid drags fluid parcels with dissolved methane into the sand layer, dispersing the methane throughout the layer.

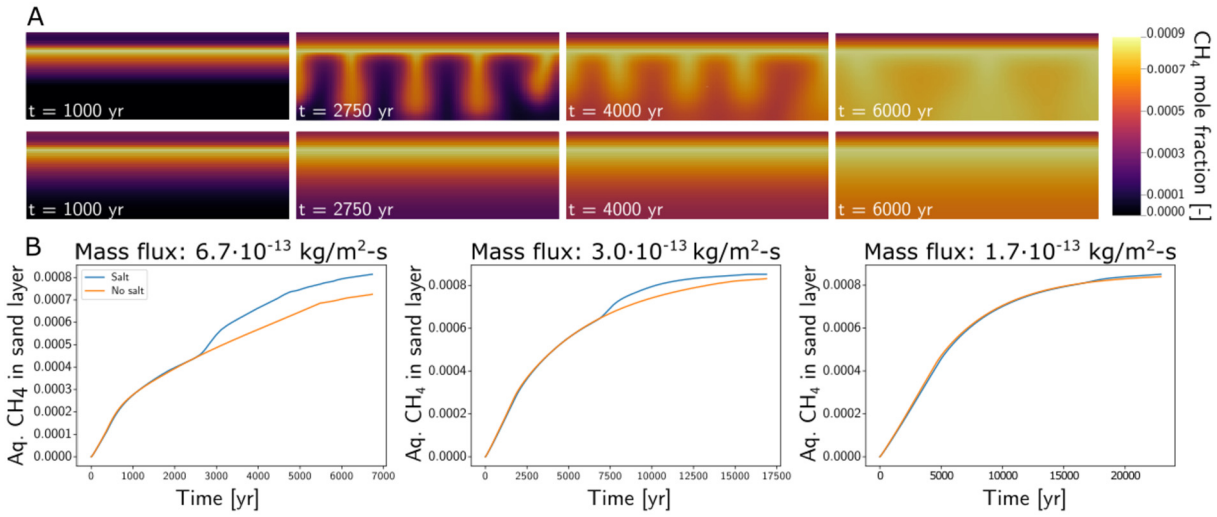

Fig. 4. (A) Convective flux (top) compared with diffusive flux (below) of aqueous methane in a system with methane entering the sand layer at the sand-clay interface at the same rate. (B) Convection transports methane throughout the layer more rapidly than diffusion. As the unstable convective contribution to the methane flux into the sands decreases, the effects of convection are reduced, with the solutions converging to the diffusive case at low methane fluxes.

6. Impact of methane generation rate on convection

The flux of aqueous methane out of the clays and into the sands controls both the rate of hydrate formation and the form that the convection takes. At a low methane flux, the hydrate formation rate is slow enough that the salt diffuses away before an instability can develop. The impact of increasing mass flux on fluid velocity and the streamlines of the fluid flow are displayed in Fig. 6. The streamlines in Fig. 6A-C demonstrate how fluid is circulated throughout the sand layer. As more hydrate forms and the instability develops, the convection cell drags fluid parcels with high concentrations of dissolved methane deep within the sand layer. The velocity of the fluid parcels is determined by the density contrast between the overlying, denser fluid, and the less dense fluid within the layer. Systems with low methane fluxes and hydrate formation rates see the formation of diffuse fingers with convective velocity less than 0.004 m/yr (Fig. 6A). With a higher methane flux, the hydrate formation rate increases, and increases the density contrast between the brine in the boundary layer and that in the sand. At increased velocities, the form of the convective fingers becomes narrower and more defined (Fig. 6B,C). Systems with high velocities also undergo a higher degree of convective mixing, characterized by the winding paths of the streamlines (Fig. 6C). At a velocity of 0.02 m/yr, the fluid parcel with dissolved methane near saturation can penetrate the entire sand layer within approximately 2500 years.

A maximum velocity is reached when the density contrast between the boundary layer and the remaining sand layer is maximized (Fig. 6D). At higher methane flux, a secondary convective instability is observed shortly following the initial convection (Fig. 6D, $6.7, 3.0 \cdot 10^{-13}$ kg m^{-2} s^{-1}). This secondary effect is less pronounced with a decreasing methane flux, and eventually disap-

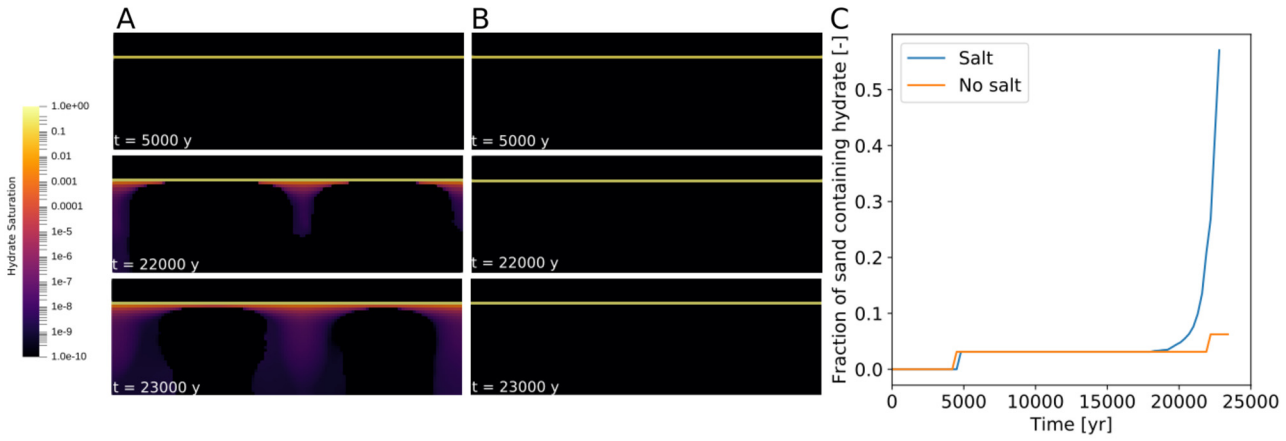

Fig. 5. Hydrate saturations developed at the clay-sand interface in systems with (A) and without salt (B). Hydrate is formed in the convective case within the finger, as methane reaches the solubility limit. Higher saturations are found where the finger develops initially. In the diffusive case, hydrate formation is largely confined to the sand-clay interface. (C) Fraction of the sand layer containing hydrate in convective (blue) and non-convective (orange) cases.

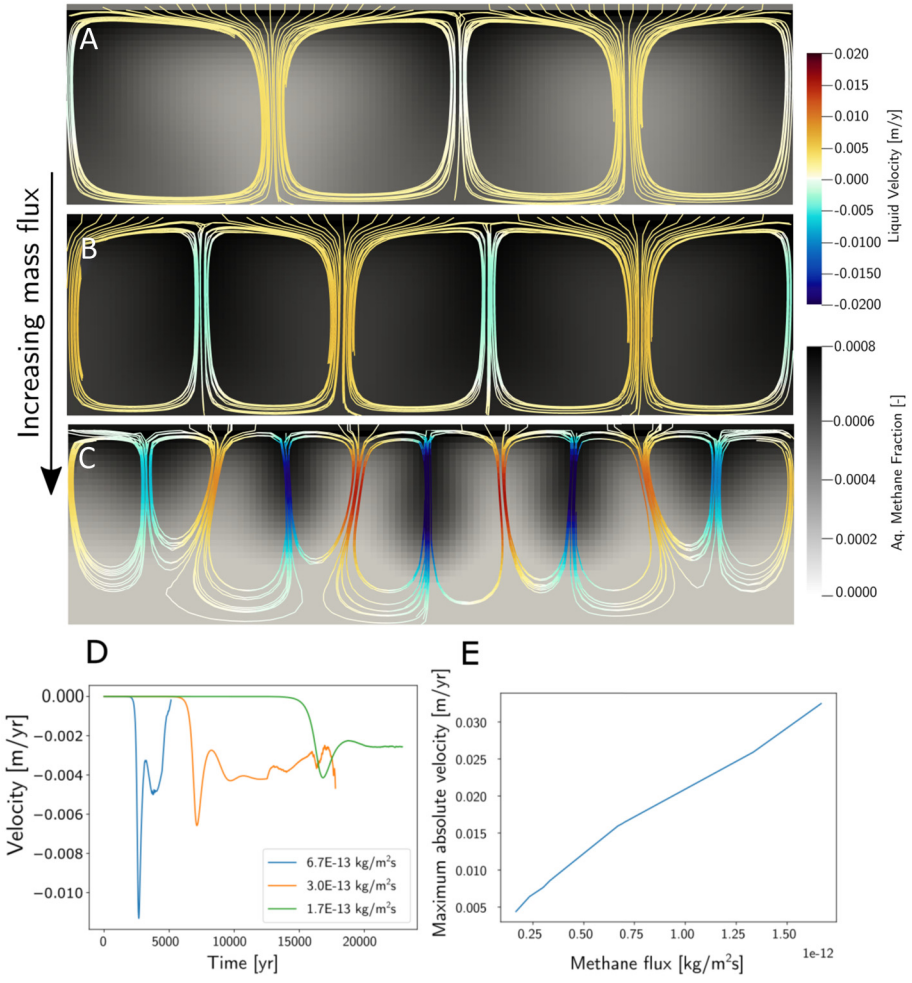

Fig. 6. Streamlines displayed over aqueous methane concentration for three different systems with methane flux decreasing from top to bottom. Faster hydrate formation leads to a greater number of fingers developed as well as a higher magnitude of velocity in the downward z direction.

pears at low fluxes. The velocity of the convection cells is a roughly linear function of the flux of methane into the system and the subsequent hydrate formation rate (Fig. 6E).

As the methane flux decreases, the fingers become wider and more diffuse, and at a flux of $1.7 \cdot 10^{-13}$ kg/m^2 s, convection does not occur and methane transport is solely diffusive. This suggests that, due to the fastest rate of methane generation occurring at shallow depths, this type of convection is most likely to occur within the first 50 m below the seafloor, where the rate of microbial methane generation is the highest.

7. Dimensionless parameters

The Rayleigh Number is a dimensionless number that describes fluid flow initiated by a density difference. In a porous medium it is defined as

$$Ra = \frac{k\Delta\rho g L}{\phi \mu D}, \tag{11}$$

where k is the permeability, $\Delta\rho$ is the density difference that initiates convection, g is the gravitational constant, L is the thickness of the sand layer, ϕ is the porosity, μ is the fluid viscosity, and D is the effective coefficient of diffusion of the solute. The Peclet number relates advective velocity to diffusivity:

$$Pe = \frac{Lu}{D}, \tag{12}$$

where u is the advective velocity.

As this system is dependent on phase change for the instability to develop, we also define a Damköhler number to account for the impact of the hydrate formation rate on the density increase. It is defined as

$$Da = \frac{k_{sh} L^2}{D\phi}, \tag{13}$$

where k_{sh} is the hydrate formation rate, and the remaining variables are the same as previously defined.

Fig. 7A shows the evolution of these three dimensionless quantities as a function of time. Due to hydrostatic pressure, the initial Ra is slightly negative, and Pe is 0 since convection has not yet initiated. The system is initially in a purely diffusive state, and diffusion remains the primary transport mechanism through the initial stages of hydrate formation. The diffusive flux throughout the layer decreases during the period of hydrate formation because methane is consumed to form hydrate. As hydrate continues to form, Ra increases until a sufficient density contrast has formed to initiate an instability and increase Pe. Ra reaches a maximum, and early convection begins. This is marked by a separation in the average mole fraction in the sand layer (Fig. 7B). Further increases in Ra lead to dampened convective pulses during late convection.

When plotting a ratio of the Peclet number to the Rayleigh number against a time variable

$$t_c = t\, Da, \tag{14}$$

where t is time, and Da is the Damköhler number defined in Eq. (14), the curves converge towards a single curve (Fig. 7C). This presents a generalizable quantity and time during which the instability forms, and the maximum early convective flux is reached. Convection occurs in hydrate systems at a ratio of Pe/Ra of 0.5, and is maximized at a t_c of 1750 years.

Studies of convection of dissolved CO_2 note the effect of Rayleigh number on finger spacing, with higher Rayleigh numbers contributing to a narrower distance between convective fingers (Riaz et al., 2006). We observe similar behavior here, with increasing mass flux resulting in a narrower finger spacing. Convective mixing in hydrate systems also share temporal similarities with CO_2 dissolution. Convection occurring from CO_2 dissolution undergoes three main stages: diffusive mixing, early convective mixing, and late convective mixing (Hassanzadeh et al., 2007). Convection induced by hydrate formation undergoes similar periods of diffusive, early convective, and late convective transport, though initiated through different means than CO_2 convection. A major difference between convection induced by hydrate formation and the convection of dissolved CO_2 is the time-dependent nature of the Ra and Pe numbers in the case of hydrate formation-induced

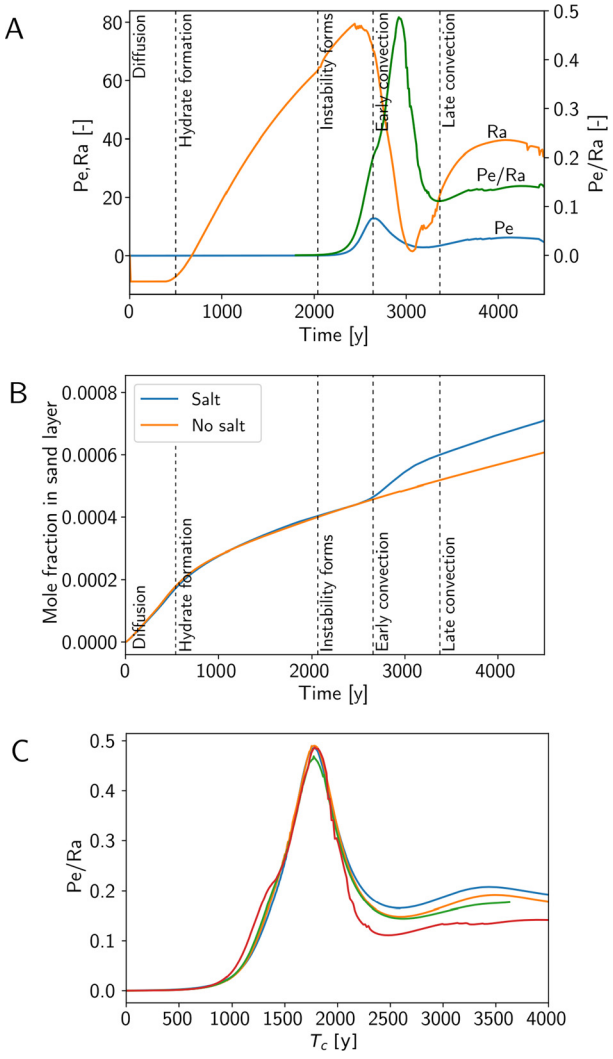

Fig. 7. (A) Stages of convection during hydrate formation. Aqueous methane transport is initially purely diffusive from the beginning through the initial stages of hydrate formation. As hydrate forms, Ra (orange) increases until an instability forms, and Pe (blue) begins to increase. Shortly after Ra is maximized, early convection begins, and Pe is maximized. Late convection begins following increases in Ra from continued hydrate formation and subsequent increases in Pe. The ratio of Pe/Ra is displayed in green. (B) Aqueous methane transport is initially purely diffusive, and the diffusive flux decreases as methane is consumed to form hydrate. Departure of the mole fraction by the convective case (Salt) from the purely diffusive case (No salt) is not observed until the early convection stage. Following the early convection stage, there is a slight decrease in the rate of aqueous methane transport into the sand layer. (C) Convection is maximized at a consistent Pe/Ra of 0.5, independent of hydrate formation rate.

convection. In the case of dissolved CO_2 convection, the aquifer geometry, diffusion coefficient, and permeability of the system can be changed to alter the patterns of convection (Hassanzadeh et al., 2007). These parameters, in addition to hydrate formation rate, alter the patterns of convection in hydrate systems. Because the solute concentration is not held constant during hydrate formation-induced convection as it is in the case of CO_2 sequestration, the Ra and Pe numbers fluctuate with time due to variation in density and velocity.

Natural convection within an infinite horizontal domain with a constant concentration upper boundary is known to occur at a critical Ra $\geq 4\pi^2$ (Bories, 1987). By varying the system geometry (Nilsen and Storesletten, 1990) or boundary conditions (Nield, 1968), the critical Ra can change. Hydrate formation-induced convection presented in this study occurs from a constant rate of methane, rather than a constant concentration of a solute, there-

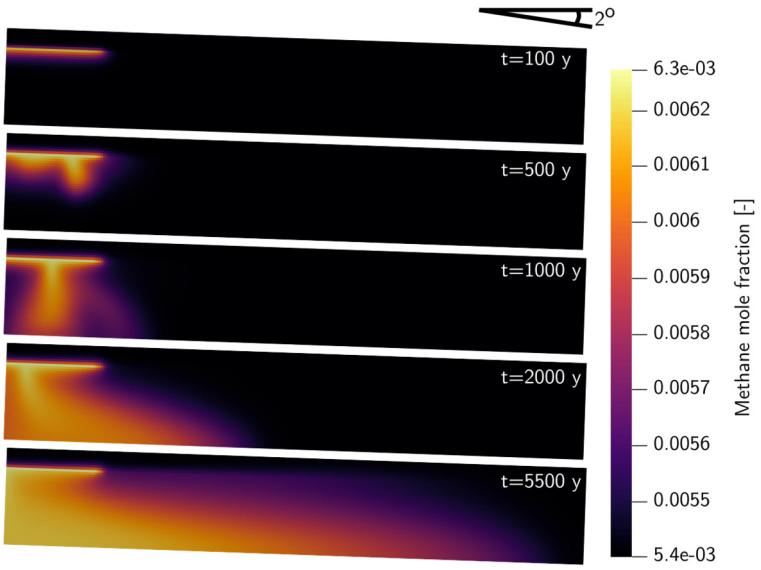

Fig. 8. Convective transport of aqueous methane in a 2° dipped layer.

fore we expect variations in the hydrate formation rate to change the critical Ra in a similar way to varying boundary conditions in the aforementioned studies of natural convection. Despite their differences, the onset of convection in CO_2 and hydrate systems are similar enough that the same dimensionless quantities can be used to inform time periods during which different transport mechanisms move dissolved components throughout the system.

8. Dipping layers

Hydrate-filled turbidite sands with dip angles as high as 25° have been found at Site WR313 in the Gulf of Mexico (Cook et al., 2012). Dipping sand layers provide a pathway for the focusing of methane-saturated fluids through varying depths, whether through overpressure that focuses methane-saturated water to shallower depths at lower methane solubility (Nole et al., 2016), through an advective gas flux (You and Flemings, 2018), or through compaction-driven flow (Frederick and Buffett, 2011). While the aforementioned studies examine advection from deep to shallow depths, density-driven convection from hydrate formation and salt exclusion acts as a mechanism for fluid focusing from shallower to deeper sediments. We show that, at even shallow dip angles of 2°, convection can focus methane-saturated fluid and promote higher accumulations of methane down-dip than would otherwise be present.

To isolate the effects of the dip, we simulated the same system as described in the previous sections, but shortened the line source to the updip 6 m of the formation. The total length of the system was set to 60 m, and the gravity vector was rotated to account for a 2 degree dip. We find that a 60 m sand layer with a dip of only 2° will have water saturated with methane reach down-dip of the observed system in only 5500 years (Fig. 8). The presence of even a slight dip greatly extends the effects of hydrate formation-driven convection. While convection in flat-lying sands is limited to the thickness of the sand layer, methane can be transported over much longer distance in dipping systems due to gravitational instability.

The geometry of the dipping layer along with the Ra number is known to host two different flow regimes at angles between 15° and 80° (Bories and Combarnous, 1973). Values of $\mathrm{Ra}\cdot\cos\theta < 4\pi^2$ develop a unicellular, two-dimensional movement occurs that diminishes the downward transport of aqueous methane, while values of $\mathrm{Ra}\cdot\cos\theta > 4\pi^2$ develop longitudinal coils parallel to the dip

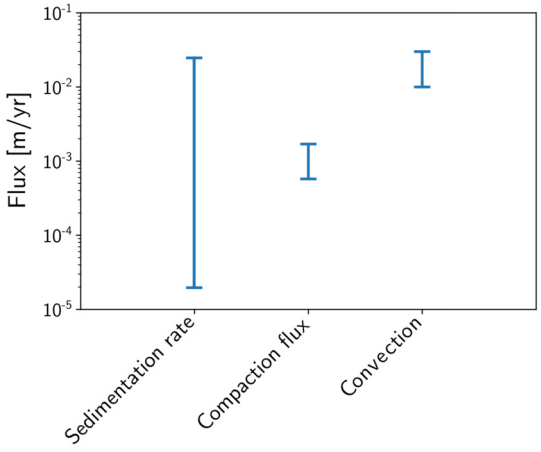

Fig. 9. Comparison of fluxes from transport processes relevant to hydrate formation in marine sediments: sedimentation, compaction, and convective flow. The density-driven convection presented in this study is rapid relative to other geologic transport processes.

of the sand layer, similar to the behavior in Fig. 8. Additionally, because the Ra in dipping layers is reduced by $\cos\theta$, the driving force may be insufficient to initiate convection at high angles, and can increase the time to initiate convection at lower angles (Javaheri et al., 2009).

Comparing the methane flux of a convective system with sedimentation rates and compaction flux demonstrates the relative importance of convection as a means of transporting methane from shallow to deeper depths (Fig. 9). Sedimentation is highly variable, with rates ranging from 10^{-4} m/yr (Akiba et al., 2009) to as high as 10^{-2} m/yr (Restreppo et al., 2020). Compaction-driven flux flows in the opposite direction of density-driven convection, and is on the order of 10^{-3} m/yr (Frederick and Buffett, 2011). At its maximum rate in the simulated scenario, density-driven convection is as fast as the most rapid sedimentation rates, with rates on the order of cm/yr. The relative rate of convection to the other fluid focusing transport mechanisms makes it a viable option for rapid transport of methane down-dip. Convective transport will, however, only work in regions without shallow overpressure. Shallow overpressure will largely overwhelm convective transfer as well as short diffusive migration.

9. Conclusions

Convective flow of pore fluid due to salt exclusion during hydrate formation is potentially a powerful mechanism for the transport of aqueous methane in geologic systems. This transport mechanism can move aqueous methane on a similar timescale to buoyant gas flows. Methane flux rates on the order of $1 \cdot 10^{-12}$ kg/m^2 s can form hydrate within a sand layer that initiates convective flows with velocities up to 0.02 m/yr. These rapid transport rates of dissolved methane can bring the sand layer to solubility much faster than a purely diffusive case. This mechanism of transport is not limited to the case of microbially-generated methane entering a sand layer from an adjacent clay layer. Convective flow of dissolved components due to hydrate formation is likely to occur in dipped layers with advection of methane gas. This work also has implications for carbon sequestration in the hydrate form, as salt exclusion and CO_2 dissolution cause convective instabilities.

CRediT authorship contribution statement

David Fukuyama: Conceptualization, Investigation, Software, Writing – original draft. **Hugh C. Daigle:** Conceptualization, Methodology, Writing – review & editing. **Michael A. Nole:** Methodology, Software, Writing – review & editing. **Wen Song:** Conceptualization, Writing – review & editing.

Declaration of competing interest

The authors declare that they have no known competing financial interests or personal relationships that could have appeared to influence the work reported in this paper.

Data availability

No data was used for the research described in the article.

Acknowledgements

This work was supported by the Laboratory Directed Research and Development program at Sandia National Laboratories. Sandia National Laboratories is a multimission laboratory managed and operated by National Technology and Engineering Solutions of Sandia, LLC., a wholly owned subsidiary of Honeywell International, Inc., for the U.S. Department of Energy's National Nuclear Security Administration under contract DE-NA-0003525. Any subjective views or opinions that might be expressed in the paper do not necessarily represent the views of the U.S. Department of Energy or the United States Government.

This article has been authored by an employee of National Technology & Engineering Solutions of Sandia, LLC under Contract No. DE-NA0003525 with the U.S. Department of Energy (DOE). The employee owns all right, title and interest in and to the article and is solely responsible for its contents. The United States Government retains and the publisher, by accepting the article for publication, acknowledges that the United States Government retains a non-exclusive, paid-up, irrevocable, world-wide license to publish or reproduce the published form of this article or allow others to do so, for United States Government purposes. The DOE will provide public access to these results of federally sponsored research in accordance with the DOE Public Access Plan https://www.energy.gov/downloads/doe-public-access-plan.

References

Akiba, F., Inoue, Y., Saito-Kato, M., Pohlman, J., 2009. Data report: diatom and foraminiferal assemblages in Pleistocene turbidite sediments from the Cascadia margin (iodp expedition 311), northeast Pacific. In: Proc. IODP – Volume, vol. 311. Citeseer, p. 2.

Batzle, M., Wang, Z., 1992. Seismic properties of pore fluids. Geophysics 57 (11), 1396–1408.

Bories, S., 1987. Natural Convection in Porous Media. Springer, Netherlands, Dordrecht, pp. 77–141.

Bories, S., Combarnous, M., 1973. Natural convection in a sloping porous layer. J. Fluid Mech. 57 (1), 63–79.

Boswell, R., Frye, M., Shelander, D., Shedd, W., McConnell, D.R., Cook, A., 2012. Architecture of gas-hydrate-bearing sands from Walker ridge 313, green canyon 955, and alaminos canyon 21: northern deepwater Gulf of Mexico. Mar. Pet. Geol. 34 (1), 134–149.

Choi, J., Kim, J.-H., Torres, M.E., Hong, W.-L., Lee, J.-W., Yi, B.Y., Bahk, J.-J., Lee, K.E., 2013. Gas origin and migration in the Ulleung basin, East sea: results from the second Ulleung basin gas hydrate drilling expedition (ubgh2). Mar. Pet. Geol. 47, 113–124.

Claypool, G.E., Milkov, A.V., Lee, Y.-J., Torres, M.E., Borowski, W.S., Tomaru, H., 2006. Microbial methane generation and gas transport in shallow sediments of an accretionary complex. Southern hydrate ridge (odp leg 204), offshore Oregon, USA.

Cook, A.E., Anderson, B.I., Rasmus, J., Sun, K., Li, Q., Collett, T.S., Goldberg, D.S., 2012. Electrical anisotropy of gas hydrate-bearing sand reservoirs in the Gulf of Mexico. Mar. Pet. Geol. 34 (1), 72–84.

Cook, A.E., Malinverno, A., 2013. Short migration of methane into a gas hydrate-bearing sand layer at Walker ridge, Gulf of Mexico. Geochem. Geophys. Geosyst. 14 (2), 283–291.

Daigle, H., Cook, A., Malinverno, A., 2015. Permeability and porosity of hydrate-bearing sediments in the northern Gulf of Mexico. Mar. Pet. Geol. 68, 551–564.

Daigle, H., Dugan, B., 2011. Permeability anisotropy and fabric development: a mechanistic explanation. Water Resour. Res. 47 (12).

Flemings, P.B., Phillips, S.C., Boswell, R., Collett, T.S., Cook, A.E., Dong, T., Frye, M., Goldberg, D.S., Guerin, G., Holland, M.E., et al., 2020. Pressure coring a Gulf of Mexico deep-water turbidite gas hydrate reservoir: initial results from the university of Texas–Gulf of Mexico 2-1 (ut-gom2-1) hydrate pressure coring expedition. Am. Assoc. Pet. Geol. Bull. 104 (9), 1847–1876.

Frederick, J.M., Buffett, B.A., 2011. Topography- and fracture-driven fluid focusing in layered ocean sediments. Geophys. Res. Lett. 38 (8).

Fukuyama, D., Daigle, H., 2020. The effect of lithologic heterogeneity on diffusive methane migration in hydrate systems. Mar. Pet. Geol. 122, 104624.

Hammond, G.E., Lichtner, P.C., Mills, R.T., 2014. Evaluating the performance of parallel subsurface simulators: an illustrative example with pflotran. Water Resour. Res. 50, 208–228.

Handa, Y., 1986. Compositions, enthalpies of dissociation, and heat capacities in the range 85 to 270 k for clathrate hydrates of methane, ethane, and propane, and enthalpy of dissociation of isobutane hydrate, as determined by a heat-flow calorimeter. J. Chem. Thermodyn. 18 (10), 915–921.

Hassanzadeh, H., Pooladi-Darvish, M., Keith, D.W., 2007. Scaling behavior of convective mixing, with application to geological storage of CO_2. AIChE J. 53 (5), 1121–1131.

Henry, P., Thomas, M., Clennell, M.B., 1999. Formation of natural gas hydrates in marine sediments: 2. Thermodynamic calculations of stability conditions in porous sediments. J. Geophys. Res., Solid Earth 104 (B10), 23005–23022.

Ito, T., Komatsu, Y., Fujii, T., Suzuki, K., Egawa, K., Nakatsuka, Y., Konno, Y., Yoneda, J., Jin, Y., Kida, M., et al., 2015. Lithological features of hydrate-bearing sediments and their relationship with gas hydrate saturation in the eastern Nankai trough, Japan. Mar. Pet. Geol. 66, 368–378.

Javaheri, M., Abedi, J., Hassanzadeh, H., 2009. Onset of convection in co2 sequestration in deep inclined saline aquifers. J. Can. Pet. Technol. 48 (08), 22–27.

Liu, X., Flemings, P.B., 2011. Capillary effects on hydrate stability in marine sediments. J. Geophys. Res., Solid Earth 116 (B7).

Malinverno, A., 2010. Marine gas hydrates in thin sand layers that soak up microbial methane. Earth Planet. Sci. Lett. 292 (3–4), 399–408.

Malinverno, A., Goldberg, D.S., 2015. Testing short-range migration of microbial methane as a hydrate formation mechanism: results from Andaman Sea and Kumano basin drill sites and global implications. Earth Planet. Sci. Lett. 422, 105–114.

Malinverno, A., Kastner, M., Torres, M., Wortmann, U., 2008. Gas hydrate occurrence from pore water chlorinity and downhole logs in a transect across the northern Cascadia margin (integrated ocean drilling program expedition 311). J. Geophys. Res., Solid Earth 113 (B8).

Nield, D., 1968. Onset of thermohaline convection in a porous medium. Water Resour. Res. 4 (3), 553–560.

Nilsen, T., Storesletten, L., 1990. An analytical study on natural convection in isotropic and anisotropic porous channels.

Nole, M., Daigle, H., Cook, A.E., Hillman, J.I., Malinverno, A., 2017. Linking basin-scale and pore-scale gas hydrate distribution patterns in diffusion-dominated marine hydrate systems. Geochem. Geophys. Geosyst. 18 (2), 653–675.

Nole, M., Daigle, H., Cook, A.E., Malinverno, A., 2016. Short-range, overpressure-driven methane migration in coarse-grained gas hydrate reservoirs. Geophys. Res. Lett. 43 (18), 9500–9508.

Rempel, A., 2011. A model for the diffusive growth of hydrate saturation anomalies in layered sediments. J. Geophys. Res., Solid Earth 116 (B10).

Restreppo, G.A., Wood, W.T., Phrampus, B.J., 2020. Oceanic sediment accumulation rates predicted via machine learning algorithm: towards sediment characterization on a global scale. Geo Mar. Lett. 40 (5), 755–763.
Riaz, A., Hesse, M., Tchelepi, H., Orr, F., 2006. Onset of convection in a gravitationally unstable diffusive boundary layer in porous media. J. Fluid Mech. 548, 87–111.
Tripathi, R., Kumar, P., Ghosh, S., Nagalingam, J., Singh, H., 2019. Culture based investigations of key microbial functional groups in gas hydrate bearing sediments of the Krishna-Godavari basin in offshore India. Mar. Pet. Geol.
Van Genuchten, M.T., 1980. A closed-form equation for predicting the hydraulic conductivity of unsaturated soils. Soil Sci. Soc. Am. J. 44 (5), 892–898.
Waite, W.F., Santamarina, J.C., Cortes, D.D., Dugan, B., Espinoza, D., Germaine, J., Jang, J., Jung, J., Kneafsey, T.J., Shin, H., et al., 2009. Physical properties of hydrate-bearing sediments. Rev. Geophys. 47 (4).
Waseda, A., Uchida, T., 2004. Origin and Migration of Methane in Gas Hydrate-Bearing Sediments in the Nankai Trough. In the Geochemical Society Special Publications, vol. 9. Elsevier, pp. 377–387.
You, K., Flemings, P.B., 2018. Methane hydrate formation in thick sandstones by free gas flow. J. Geophys. Res., Solid Earth 123 (6), 4582–4600.
You, K., Flemings, P.B., Malinverno, A., Collett, T., Darnell, K., 2019. Mechanisms of methane hydrate formation in geological systems. Rev. Geophys. 57 (4), 1146–1196.